4. Groisman, P. Ya, Karl, T. R. & Knight, T. W. Observed impact of snow cover on the heat balance and the rise of continental spring temperatures. *Science* **263,** 198–200 (1994).
5. Tucker, C. J. in *Advances in the Use of NOAA AVHRR Data for Land Applications* (ed. D'Souza, D.) 1–19 (European Economic Union Press, Brussells, 1995).
6. James, M. E. & Kalluri, S. N. V. The Pathfinder AVHRR land data set: an improved coarse-resolution data set for terrestrial monitoring. *Int. J. Remote Sens.* **15,** 3347–3364 (1994).
7. Tucker, C. J., Fung, I. Y., Keeling, C. D. & Gammon, R. H. Relationship between atmospheric CO_2 variations and a satellite-derived vegetation index. *Nature* **319,** 195–199 (1986).
8. Asrar, G., Fuchs, M., Kanemasu, E. T. & Hatfield, J. L. Estimating absorbed photosynthetic radiation and leaf area index from spectral reflectance in wheat. *Agron. J.* **76,** 300–306 (1984).
9. Myneni, R. B., Hall, F. G., Sellers, P. J. & Marshak, A. L. the interpretation of spectral vegetation indexes. *IEEE Trans. Geosci. Remote Sens.* **33,** 481–486 (1995).
10. Tucker, C. J., Newcomb, W. W. & Dregne, A. E. AVHRR data sets for determination of desert spatial extent. *Int. J. Remote Sens.* **15,** 3547–3566 (1994).
11. Rao, C. R. N. & Chen, J. Inter-satellite calibration linkages for the visible and near-infrared channels of the advanced Very High Resolution Radiometer on the NOAA-7, -9, and -11 spacecraft. *Int. J. Remote Sens.* **16,** 1931–1942 (1995).
12. Los, S. O. Calibration adjustment of the NOAA AVHR Normalized Difference Vegetation Index without recourse to component channel 1 and 2 data. *Int. J. Remote Sens.* **14,** 1907–1917 (1993).
13. Holben, B. N. Characteristics of maximum value composite images for temporal AVHRR data. *Int. J. Remote Sens.* **7,** 1417–1437 (1986).
14. Myneni, R. B., Tucker, C. J., Asrar, G., Keeling, C. D. & Nemani, R. R. Increased vegetation greenness amplitude and growing season duration in northern high latitudes inferred from satellite-sensed vegetation index data from 1981–91. *NASA Tech. Memo. 104638* (NASA Goddard Space Flight Center, Greenbelt, MD, 1996).
15. Myneni, R. B., Los, S. & Tucker, C. J. Satellite-based identification of linked vegetation index and sea surface temperature anomaly areas from 1982–1990 for Africa, Australia and South America. *Geophys. Res. Lett.* **23,** 729–732 (1996).
16. Keeling, C. D., Whorf, T. P., Wahlen, M. & van der Plicht, J. Interannual extremes in the rate of rise of atmospheric carbon dioxide since 1980. *Nature* **375,** 666–670 (1995).
17. Heimann, M., Keeling, C. D. & Tucker, C. J. in *Aspects of Climate Variability in the Pacific and Western Americas* (ed. Peterson, D. H.) 277–303 (Geophys. Monog. Ser., Am. Geophys. Union, Washington DC, 1989).
18. Kauppi, P. E., Mielikainen, K. & Kuusela, K. Biomass and carbon budget of European forests from 1971–1990. *Science* **256,** 70–74 (1992).
19. Jacoby, G. C., D'Arrigo, R. D. & Davaajamts, T. Mongolian tree rings and 20th-century warming. *Science* **273,** 771–773 (1996).
20. Houghton, J. T. *et al.* (eds) *Climate Change 1995* 1–365 (Cambridge Univ. Press, 1995).
21. Jones, P. D., Wigley, T. M. L. & Briffa, K. R. in *Trends '93: A Compendium of Data on Global Change* (eds Boden, T. A., Kaiser, D. P., Sepanski, R. J. & Stoss, F. W.) (ORNL/CDIAC-65, Oak Ridge, TN, 1994).
22. Piper, S. C. & Stewart, E. F. A gridded global data set of daily temperature and precipitation for terrestrial biosphere modelling. *Glob. Biogeochem. Cycles* **10,** 757–782 (1996).

Acknowledgements. We thank S. C. Piper and E. F. Stewart for analysis of the station temperature data, S. C. Piper and T. P. Whorf for discussions, and S. Los for help in the calibration of GIMMS NDVI data. This work was supported by the Office of Mission ot Planet Earth of NASA. E. F. Stewart's collaboration was made possible by funds from the Electric Power Research Institute and the USNSF.

Correspondence should be addressed to R.B.M. (e-mail: rmyneni@crsa.bu.edu).

Large-scale tectonic deformation inferred from small earthquakes

Falk Amelung* & Geoffrey King

Institut de Physique du Globe, 5, Rue Rene Descartes, F-67084 Strasbourg, France

It is a long-standing question whether the focal mechanisms of small earthquakes can be used to provide information about tectonic deformation on a regional scale. Here we address this question by using a 28-year record of seismicity in the San Francisco Bay area to compare the strain released by small earthquakes with geological, geodetic and plate-tectonic measurements of deformation in this region. We show that on a small spatial scale, the strain released by small earthquakes is closely related to specific geological features. But when averaged over a regional scale, strain release more closely follows the regional pattern of tectonic deformation: this relationship holds for all but the largest earthquakes, indicating that the earthquake strain is self-similar[1,2] over a broad range of earthquake magnitudes. The lack of self-similarity observed for the largest earthquakes suggests that the time interval studied is not large enough to sample a complete set of events—the fault with the highest probability[3] for hosting one such missing event is the Hayward fault.

* Present addresses: Department of Geophysics, Stanford University, Stanford, California 94305, USA (F.A.); Institut de Physique du Globe, Laboratoire de Tectonique, Tour 24, BP89, 4 Place Jussieu, 75252 Paris, France (G.K.).

Following the formulation by Kostrov[4], the seismic strain of a block in the Earth's crust can be obtained from the geometric moment tensors

$$\epsilon_{ij} = \frac{1}{2V}\sum_{n=1}^{N} \mathcal{M}_{ij}^{(n)} \qquad (1)$$

where $\mathcal{M}_{ij}^{(n)}$ is the geometric moment tensor of the nth earthquake, N is the number of earthquakes and V is the volume of the block. The geometric moment tensor of an earthquake is given by $\mathcal{M}_{ij} = \int_A u\mathrm{d}A(u_i n_j + u_j n_i)$, where A is the surface of the fault, dA is a surface element, u is the slip in the earthquake, and u_i and n_i are the unit slip and fault-normal vectors, respectively. The geometric moment tensor $\mathcal{M}_{ij}$, referred to by Ben-Menahem and Singh[5] as "potency", is related to the seismic moment tensor M_{ij} used in seismology by $M_{ij} = \mu\mathcal{M}_{ij}$ (ref. 6), where μ is the shear modulus.

The strain in a local region, $\epsilon_{ij}^{(\mathrm{loc})}$, is related to the strain in a larger region, $\epsilon_{ij}^{(\mathrm{reg})}$, by a fourth-order tensor that is a complicated function of time and space. Here we consider special cases in which they are assumed to be linearly related by

$$\epsilon_{ij}^{(\mathrm{loc})} = c\epsilon_{ij}^{(\mathrm{reg})} \qquad (2)$$

where c is the amplitude of the local deformation, that is, the shape and the orientation of the local and regional strain tensors are identical but their amplitudes can be different. For homogeneous deformation, $c = 1$. If seismic strain is self-similar and if $\epsilon_{ij}^{(\mathrm{loc})}$ is the seismic strain by earthquakes in one scale, then equation (2) will apply at any scale with different values for c. Some examples are

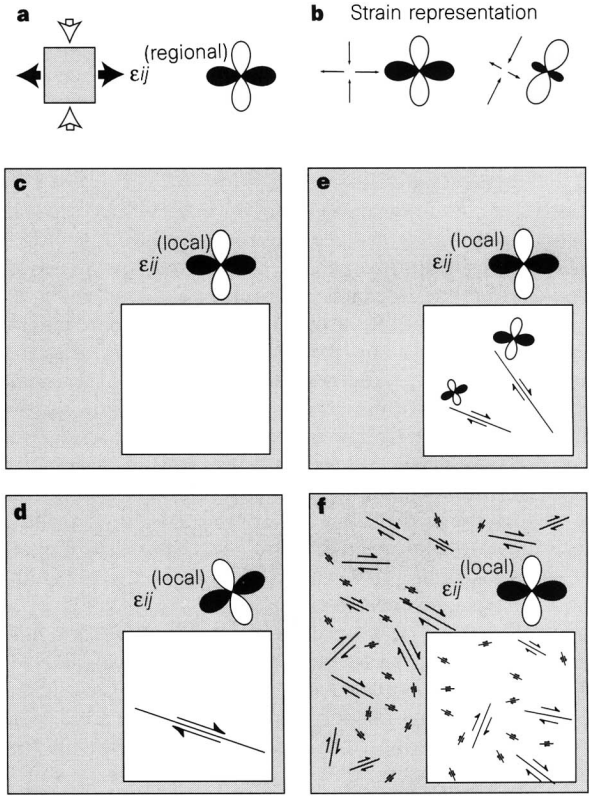

Figure 1 Homogeneous and inhomogeneous deformation in four different regions subject to pure shear. **a**, Boundary conditions and imposed strain. **b**, The strain tensor is represented by two-dimensional strain rosettes for the horizontal components. White lobes indicate directions of contraction, black lobes indicate directions of extensions. **c**, Homogeneous deformation. **d**, Inhomogeneous deformation due to an individual shear fault. **e**, Inhomogeneous deformation due to two faults. **f**, Quasi-homogeneous deformation due to many shear faults with a variety of orientations.

illustrated in Fig. 1. The (applied) regional strain is pure shear (Fig. 1a). We refer to the orientation and shape of a strain tensor as the strain pattern and use strain rosettes for the representation (Fig. 1b). In the absence of faults the strain is homogeneous and the strain pattern in a local region is identical to the regional strain (Fig. 1c). The strain due to slip on a single fault is in general different from the regional strain (Fig. 1d). Two shear faults are, in principle, sufficient to accommodate any regional shear although strain concentrations can be large (Fig. 1e). The strain pattern in a region that contains many faults with a variety of orientations and homogeneous spatial distribution tends to equal the regional strain (Fig. 1f). Note that Fig. 1f is identical to Fig. 1c if the faults are small compared to the dimension of the region.

The larger San Francisco Bay area (Fig. 3a) is part of the plate boundary zone between the Pacific and North American plates. The regional deformation is primarily simple shear. South of 37° N nearly all the transform motion is accommodated on the San Andreas fault and the motion is mainly aseismic (creeping section).

Table 1 Seismic deformation in earthquake regions

Region	Direction of principal contraction	$\frac{\lvert\text{principal extensional}\rvert}{\lvert\text{principal contraction}\rvert}$	Number of events summed
Golden Gate	N3°W	2.9	58
San Francisco Peninsula	N31°W	0.29	170
Loma Prieta	N16°W	0.57	885
Hollister	N3°W	0.91	7,117
Calaveras fault	N14°W	0.99	2,303
Hayward fault	N12°W	0.88	341
Livermore	N33°W	1	1,239
San Gregorio fault	N20°W	0.59	75
North Bay	N28°W	0.77	98
Diablo Range	N26°W	0.77	182

Shown here are the directions of principal contraction and ratios between the principal components of the horizontal strain in the regions from Fig. 3, for all events with magnitude ≤ 3.33.

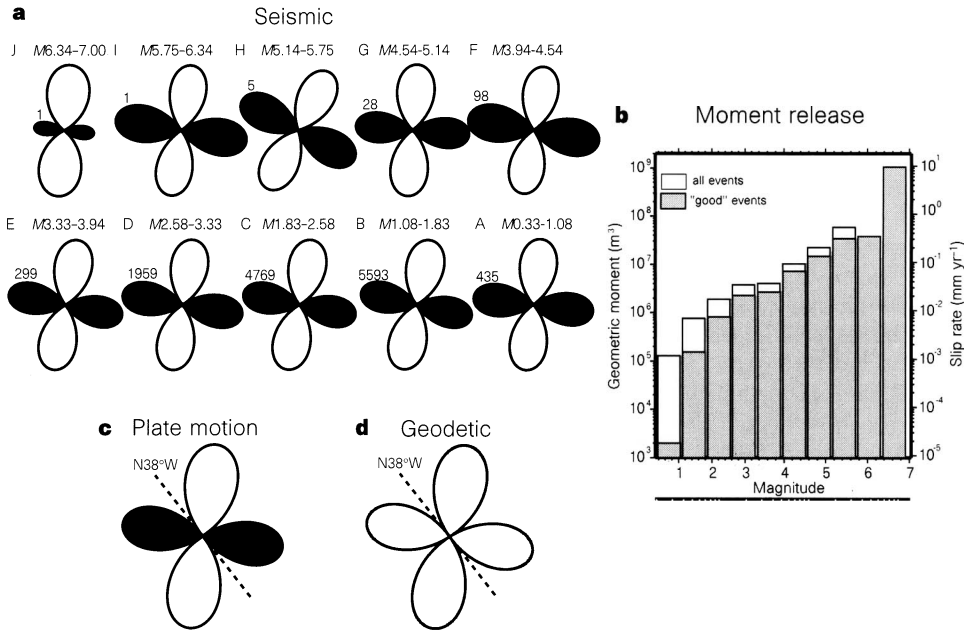

Figure 2 a, Two-dimensional strain rosettes representing the horizontal seismic strain patterns due to the earthquakes in Fig. 3 in magnitude ranges for which mean fault dimensions differ by factors of 2 (A–J). The numbers of events summed are shown next to the strain rosettes. The fault plane solutions are calculated from the first motion polarities using the computer program FPFIT[32]. The geometric moments are calculated for the local or duration magnitude, M, using the empirical relations $\log M_0 = 1.5M - 1.5$ for $M > 3.33$ and $\log M_0 = 1.2M - 0.5$ for $M \leq 3.33$ (modified from Bakun's[33] relations for the seismic moment using $\mu = 30$ GPa). In this study only "good" events satisfying some quality criteria are used; with uncertainties in strike, dip and rake less than 30°, 45° and 45°, and with magnitude ≥ 0.3, depth ≥ 2 km, r.m.s. ≤ 0.3 s; horizontal location error ≤ 2.5 km; vertical location error ≤ 5 km; number of first motions ≥ 30; azimuthal gap ≤ 180° (see ref. 32 for explanation of these parameters) %rtp ≤ 0.4; sdr ≥ 0.4; fit ≤ 0.4. **b**, Summed geometric moment within the magnitude intervals. The fault length is for circular faults and displacement-to-length ratios of 3×10^{-4}. The abscissa is not linear in magnitude because of two different moment–magnitude relations. The slip rate contribution is averaged over the observational period of 28 years and assumes that the events fall on a 250-km-long and 15-km-deep plate boundary fault. **c**, Predicted strain pattern for an orientation of the Pacific–North American plate boundary of N38° W, and relative motion of the Pacific plate in N34° W. **d**, Mean geodetic strain pattern from trilateration data[16]. The contributions of the San Francisco Bay network and of the Monterey network are summed. It is assumed that they cover three-quarters and one-quarter of the region studied, respectively. The strain rosettes in **c** and **d** represent 5% contraction perpendicular to N38° W.

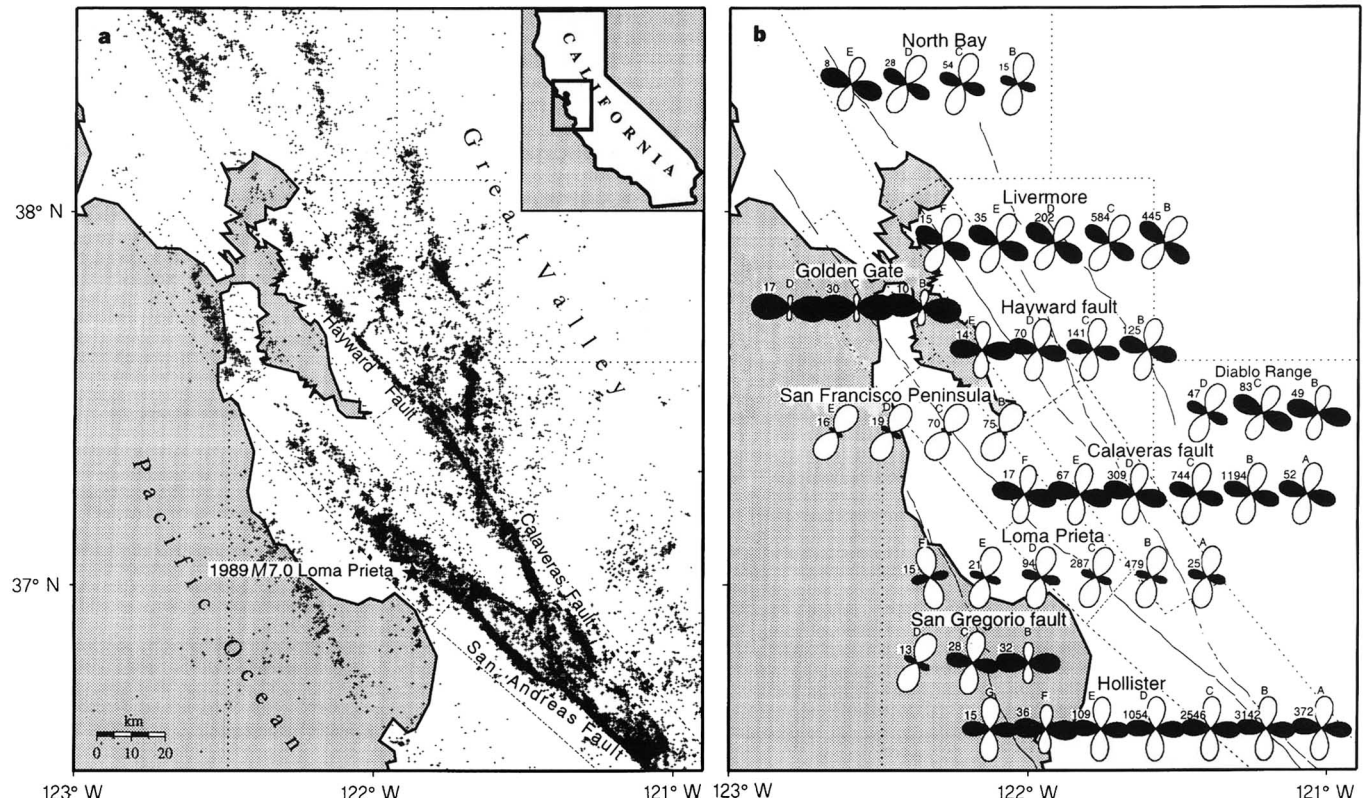

Figure 3 a, Location map showing the seismicity ($M > 1.0$) registered by the Northern Californian Seismic Network (NCSN) between January 1968 and December 1995 in the broader San Francisco Bay area. This study uses 15% of the 95,000 registered events with well constrained moment tensors. **b**, Two-dimensional strain rosettes representing the horizontal strain due to earthquakes in the magnitude ranges defined in Fig. 2a (denoted by letters A–G). Only strain rosettes resulting from summing >5 events are shown. The numbers of events summed are shown next to the strain rosettes.

Further north, two-thirds of the deformation[7] occurs on the San Andreas fault in occasional large earthquakes such as the 400-km-long rupture in 1906 or in smaller earthquakes that rupture fault segments 10–40 km long[3]. The remaining deformation is accommodated on subparallel strike-slip faults. The Hayward fault, for example, has been the source of two earthquakes with magnitudes (M) between 6.5 and 7 in 1836 and 1868 (ref. 8), and the Calaveras fault has ruptured in a sequence of earthquakes with $M > 5.5$ beginning in 1979; the $M = 6.2$ 1984 Morgan Hill earthquake was the largest[9,10]. The recurrence times of 1906-type San Francisco earthquakes, of events on the Hayward fault and the Calaveras fault earthquakes are of the order of 250 years, 150 years and 80 years, respectively[3]. The seismic data covers a 28-year time period, which is nearly one-third of the shortest seismic cycle.

The seismic deformation of the San Francisco Bay area for different magnitude intervals is shown in Fig. 2a. The geometric moment tensors are derived from the fault plane solution and the magnitude for each event. The magnitude ranges have been chosen such that the seismic moments vary from one range to the other by a factor of 8. For events that are individually self-similar this corresponds to a factor of 2 change in mean fault dimensions between ranges[11–13]. It can be seen that the strain patterns in the magnitude intervals below magnitude 3.94 are similar and can be interpreted as right-lateral shear across N38° W and 5% of shortening in perpendicular direction. The strain patterns differ only for the largest earthquakes where few events have been summed. The similarity of the strain patterns, together with the fact that the events occurred in different parts of the Bay area on faults with different orientations, suggests that the small faults slipped such that the ensemble resulted in a homogeneous reduction of elastic strain. If that is true, equation (2) is satisfied and the strain accommodated by small earthquakes represents the applied deformation. The similarity of the strain patterns also indicates the self-similarity of earthquake strain. As many other aspects of rupture of rock are self-similar phenomena, such a self-similarity is expected to occur. Although the strain patterns for different magnitude ranges are similar, the strain amplitudes vary strongly. This can be seen in Fig. 2b where the summed release of geometric moment is shown. The nearly linear increase of the summed moment with the fault length is characteristic for tectonic environments with a b-value (the slope in the Gutenberg–Richter frquency of earthquake-occurrence relation) of ~1.0 (refs 14, 15). Note that the summed moment released by all the earthquakes and that by the 'good' earthquakes (with source parameters satisfying some quality criteria) are similar except in the two lowest magnitude intervals. The appropriateness of the quality criteria has been checked by examining the stability of all the seismic strain patterns obtained in this study using more and less strict criteria.

The seismic strain pattern can be compared with the strain pattern from plate motion and from geodetic[16] information (Fig. 2c, d). The plate motion strain pattern is calculated from the relative velocity between the plates and the plate boundary direction, along which linear deformation is assumed not to occur[17]. According to plate motion models, the Pacific plate at the latitude of San Francisco moves N34° W with respect to North America[18,19]. For a plate boundary direction of N34° W, the San Francisco Bay area would shear right-laterally at N34° W. The average strike of the major strike-slip faults, however, is more westerly. For a plate boundary direction of N38° W the predicted mean deformation contains some boundary normal contraction.

The good agreement between the seismic strain patterns in the lower magnitude intervals ($M = 0.33$–3.94), and the strain patterns

from the plate motion and from geodesy clearly shows that the deformation by the small earthquakes is in direction identical to the applied deformation, that is, the seismic (local) deformation and the applied (regional) deformation are linearly related by equation (2). The condition for this to be true appears to be that a sufficient number of earthquakes with comparable size and on faults with a variety of orientations are summed. If not, the deformation will be different because some event types are missing. This is the case for the higher magnitude intervals. In the $M = 3.94$–6.34 range, some earthquakes with a significant reverse component are absent. In the $M = 6.34$–7.00 range, a strike-slip event is missing. The fault with the highest probability[3] for such an earthquake is the Hayward fault.

We note at this stage that the seismic strain pattern, the predicted strain pattern, as well as the geodetic strain pattern imply that, in the San Francisco Bay area, a shortening of ~5% of the shear deformation (2 mm yr^{-1}) occurs normal to the plate boundary (assumed to be oriented N38° W). This is indicated by various geological and geophysical evidence[20–23], but has been questioned because the geodetic data has been interpreted differently[16,24]. (Those studies examined the geodetic data for shortening perpendicular to the plate motion direction (N34° W) and not perpendicular to the plate boundary direction (N38° W).)

So far this study has been concerned with the overall deformation across the entire San Francisco Bay area (Fig. 3a). Figure 3b shows that within the Bay area the seismic deformation varies locally (see also Table 1). In almost all local regions the strain patterns are independent of earthquake size. A comparison with the geodetic strain pattern in these small areas is difficult because the geodetic data lacks sufficient resolution[25]. The seismic strain patterns, however, are associated with local tectonics and can partly be predicted from the geometry of the major strike-slip faults. In regions where they are oriented in the plate motion direction we expect shear, as observed for example in the Calaveras area. In regions where the trend of the faults is more westerly or more easterly we expect net contraction or net extension. This is observed along the San Andreas fault. In the San Francisco Peninsula, the Loma Prieta and the Hollister regions (although less prominent there), where the fault strikes more westerly than the plate motion, the seismic strain is contractional. Around the Golden Gate, where the fault strikes more easterly, the seismic strain is extensional. These strain patterns are compatible with the uplift of the southern Santa Cruz Mountains and the subsidence of the Golden Gate area, respectively[25].

Earthquake focal mechanisms are commonly interpreted with respect to the state of stress in the Earth's crust[26–28]. Here we have been concerned with the state of strain. In homogeneous, isotropic material the elastic strain results in a stress state with identical principal directions. In the Earth's brittle crust, however, they should be different because the strain localizes on fractures or faults on a range of scales. In determining strain by summing over many events and over a large period of time we average over strain heterogeneities and reproduce the applied deformation. Stress inversion assumes that the earthquakes are driven by a single stress tensor invariant in space and time, and if the same strain and stress directions are obtained from focal mechanism data this is fortuitous. In the Loma Prieta region, for example, the strain directions differ from stress directions previously reported[29–31], possibly because the hypothesis of a spatially and temporally uniform stress tensor is not met. □

Received 2 August 1996; accepted 21 February 1997.

1. Mandelbrot, B. B. *The Fractal Geometry of Nature* (Freeman, San Francisco, 1983).
2. Turcotte, D. L. *Fractals and Chaos in Geology and Geophysics* (Cambridge Univ. Press, Cambridge, 1992).
3. Working Group on Californian Earthquake Probabilities *Probabilities of Large Earthquakes in the San Francisco Bay Region, California* (Circ. 1053, US Geol. Survey, 1990).
4. Kostrov, V. V. *Earth Phys.* **1,** 23–40 (1974).
5. Ben-Menahem, A. & Singh, J. J. *Seismic Waves and Sources* (Springer, New York, 1981).
6. King, G. C. P. *Phil. Trans. R. Soc. Lond. A* **288,** 197–212 (1978).
7. Kelson, K. I., Lettis, W. R. & Lisowski, M. *Proc. 2nd Conf. on Earthquake Hazards in the Eastern San Francisco Bay Area* 31–38 (Spec. Publ. 113, California Dept. of Conservation, Div. of Mines and Geology, 1992).
8. Ellsworth, W. *Prof. Pap. US Geol. Surv.* **1515,** 153–181 (1990).
9. Oppenheimer, D. H., Reasenberg, P. A. & Simpson, R. W. *J. Geophys. Res.* **93,** 9007–9026 (1988).
10. Oppenheimer, D. H., Bakun, W. H. & Lindh, A. G. *J. Geophys. Res.* **95,** 8483–8489 (1990).
11. Bakun, W. H., King, G. C. P. & Cockerham, R. S. in *Earthquake Source Mechanics* 195–207 (Geophys. Monogr. 37, (Maurice Ewing 6), Am. Geophys. Union, 1986).
12. King, G. C. P., Lindh, A. G. & Oppenheimer, D. H. *Geophys. Res. Lett.* **17,** 1449–1452 (1990).
13. King, G. C. P., Oppenheimer, D. & Amelung, F. *Earth Planet. Sci. Lett.* **128,** 55–64 (1994).
14. King, G. C. P. *Pure Appl. Geophys.* **121,** 761–815 (1983).
15. Amelung, F. & King, G. C. P. *Geophys. Res. Lett.* **24,** 507–510 (1997).
16. Lisowski, M., Savage, J. C. & Prescott, W. H. *J. Geophys. Res.* **96,** 8369–8389 (1991).
17. Ekström, G. & England, P. *J. Geophys. Res.* **94,** 10231–10257 (1989).
18. DeMets, C., Gordon, R. G., Argus, D. F. & Stein, S. *Geophys. J. Int.* **101,** 425–478 (1990).
19. DeMets, C., Gordon, R. G., Argus, D. F. & Stein, S. *Geophys. Res. Lett.* **21,** 2191–2194 (1994).
20. Page, B. M. in *Proc. 2nd Conf. on Earthquake Hazards in the Eastern San Francisco Bay Area* 1–7 (Spec. Publ. 113, California Dept. of Conservation, Div. of Mines and Geology, 1992).
21. Page, B. M. & Brocher, T. M. *Geology* **21,** 635–638 (1993).
22. Jones, D. L. *et al. Tectonics* **13,** 561–574 (1994).
23. Zoback, M. D. *et al. Science* **238,** 1105–1111 (1987).
24. Williams, S. D. P. thesis, Univ. Durham (1995).
25. Amelung, F. thesis, Univ. Louis Pasteur, Strasbourg (1996).
26. Gephart, J. W. & D. W. Forsyth *J. Geophys. Res.* **89,** 9305–9320 (1984).
27. Michael, A. J. *J. Geophys. Res.* **89,** 11517–11526 (1984).
28. Rivera, L. & Cisternas, A. *Bull. Seismol. Soc. Am.* **80,** 600–614 (1990).
29. Michael, A. J., Ellsworth, W. L. & Oppenheimer, D. H. *Geophy. Res. Lett.* **17,** 1441–1444 (1990).
30. Beroza, G. C. & Zoback, M. D. *Science* **259,** 210–213 (1993).
31. Zoback, M. D. & Beroza, G. C. *Geology* **21,** 181–185 (1993).
32. Reasenberg, P. A. & Oppenheimer, D. H. *US Geol. Surv. Open-File Rep.* **85-739** (1985).
33. Bakun, W. H. *Bull. Seismol. Soc. Am.* **74,** 439–458 (1984).

Acknowledgements. We thank D. Oppenheimer for help with the data. This work was supported by the CNRS. F.A. was supported by the EU EPOCH programme.

Correspondence should be addressed to F.A.

A snake with legs from the marine Cretaceous of the Middle East

Michael W. Caldwell* & Michael S. Y. Lee†

* *Department of Geology, The Field Museum, Roosevelt Road at Lakeshore Drive, Chicago, Illinois 60605, USA and Department of Biological Science, Biological Sciences Center, University of Alberta, Edmonton, Alberta T6G 2E9, Canada*
† *Zoology Building, School of Biological Sciences, The University of Sydney, NSW 2006, Australia*

Although snakes are descended from limbed squamates ('lizards'), all known snakes lack well developed legs and their nearest lizard relatives have yet to be identified[1–4]. Here we provide compelling evidence that the Cretaceous squamate *Pachyrhachis problematicus*, previously interpreted as a varanoid lizard[5–7], is actually a primitive snake with a well developed pelvis and hindlimbs. *Pachyrhachis* is the sister-taxon of all other snakes. The skull exhibits most derived features of modern snakes, and the body is slender and elongated. But unlike other snakes, *Pachyrhachis* retains a well developed sacrum, pelvis and hindlimb (femur, tibia, fibula, tarsals). *Pachyrhachis* was marine, and provides additional support for mosasauroid–snake affinities.

Both specimens of *Pachyrhachis problematicus* were found in limestone quarries at Ein Jabrud (Bed-Meir Formation, lowermost Cenomanian, mid-Cretaceous[8]), 20 km north of Jerusalem, Israel. The first was named *Pachyrhachis problematicus* (HUJ-PAL 3569)[5,6] and the second *Ophiomorphus colberti* (HUJ-PAL 3775)[7]. *Ophiomorphus* was pre-occupied, and thus changed to *Estesius*[9]. Some snake-like features were noted in both but it was concluded that they were long-bodied varanoid lizards and probably not closely related to snakes[6,7]. Our re-study found no significant differences between the two specimens (Figs 1 and 2). The posterior region of *Pachyrhachis* is not preserved, resulting in the reported absence of the hindlimb[7] (Fig. 3). *Pachyrhachis* is slightly larger and